Shelled Drone with Meshed Net Performance Evaluation through Aerodynamic Analysis and Vibration Response Investigation

Jeanette Pao, *Member, IAENG,* Carl John Salaan, *Member, IAENG,* Charles Alver Banglos, Karl Martin Aldueso, Lester Librado, and Jonathan Maglasang, *Member, IAENG*

***Abstract*—For infrastructure inspections, shelled drones have efficiently and effectively visually inspected various infrastructures, giving good visual conditions and increasing motion effectiveness. In bridge inspection, shelled drones can encounter another problem considering the presence of wind. Improving the flight performance by reducing the overall drag means decreasing the overall area of the shell. However, this could danger the drone because of the larger extrusions of the protective shell component. Thus, adding meshed net further augments the safety and survivability of the shelled drone.**

An aerodynamic investigation was conducted through Computational Fluid Dynamic (CFD) simulations and wind tunnel experiments. The addition of meshed net increased the drag force of the shelled drone by 1.52% for the ordinary nylon material and 1.61% for the braided fishing line material. The added meshed net gives only an average value of 1.56% drag contribution for any meshed net material type for the shelled drone. Moreover, reduced overall drag force was attained at increasing sideslip angle application.

For bridge inspections, shelled drones will experience significant vibrations due to wind. Thus, the wind tunnel experiment and actual flight test investigated the shelled drone with meshed net vibration response. Based on the evaluation, the shell with any material of meshed net showed system stability. The shell with its monofilament nylon meshed net indicated lower amplitude values, giving a better vibration response than the shell of other meshed net material. The actual flight test in the bridge was made and further verified the performance of the shelled drone with the monofilament nylon meshed net.

***Index Terms*—aerodynamics, bridge inspection, shelled drone, CFD simulation, spherical shell, vibration, stability.**

I. Introduction

DRONES are being used for infrastructure inspections and employed in the surveillance field for indoor and outdoor spaces [1]. Nowadays, shelled drones have efficiently and effectively visually inspected various infrastructures that provide safety inspection, convenience, and pre-inspection information.

Manuscript received May 15, 2022; revised November 2, 2022.

J. Pao is a graduate student of Mindanao State University – Iligan Institute of Technology, Iligan City, Philippines (e-mail: jeanette.pao@g.msuiit.edu.ph).

C. J. Salaan is a professor of Electrical Engineering and Technology Department, Mindanao State University – Iligan Institute of Technology, Iligan City, Philippines (e-mail: carljohn.salaan@g.msuiit.edu.ph).

C. A. Banglos is a researcher of Mindanao State University – Iligan Institute of Technology, Iligan City, Philippines (e-mail: charlesalver.banglos@g.msuiit.edu.ph).

K. M. Aldueso is a professor of Electrical Engineering and Technology Department, Mindanao State University – Iligan Institute of Technology, Iligan City, Philippines (e-mail: karlmartin.aldueso@g.msuiit.edu.ph).

L. Librado is a lecturer of Mindanao State University – Iligan Institute of Technology, Iligan City, Philippines (e-mail: lester.librado@g.msuiit.edu.ph).

J. Maglasang is a director and professor of Mechanical and Aerospace Engineering at Cebu Technological University, Cebu City, Philippines (e-mail: jonathan.maglasang@ctu.edu.ph).

Fig. 1. Shelled drone with meshed net used in bridge inspection

Obstacle-avoidance techniques for shelled drones, especially in narrow or complex environments such as damaged infrastructures [2], [3], addressed this problem. An obstacle-avoidance method such as distance or vision sensors [4], [5], [6], [7] make obstacles too complex to detect, thus resulting in unavoidable collisions. Adding a protective shell that encloses the drone inside [8], [9], [10], [11] addresses the collision problem while giving a good visual condition and increasing motion effectiveness. There is no risk of propeller damage because they are protected. Most shells of drones are in the form of a sphere that is passive rotating, which enables the drone to collide with obstacles without compromising its flight stability [12], [13], [14], [15].

The protective shell contributes to the overall drag force; thus, improvising the 3V geodesic dome is an interesting method. Fullerene-type structured spherical shells with airfoil-type joints lessened the overall drag force and improved the drone flight performance [16]. A fullerene-type spherical shell is a type of shell in the form of a 3V geodesic dome with removed connections. However, due to the removed connections to form the fullerene-type shell, it may still cause danger to the drone due to unwanted materials that could enter during an inspection.

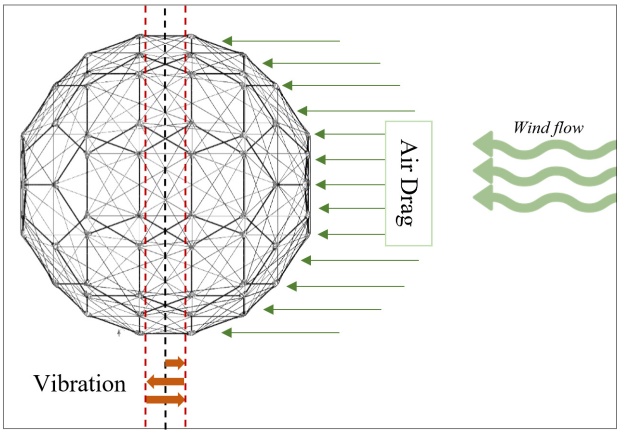

Fig. 2. Drag and vibration effect on the spherical shell due to the presence of wind during bridge inspections

Previous studies focus on protecting the drone using a passive rotating spherical shell. And some studies removed some parts of the spherical shell to reduce the drag force and overall weight, forming the fullerene-type spherical shell. Removing these parts results in larger openings that may danger the drone. The prospective solution for the current problem is the additional protection for the shelled drone by adding meshed net based on recent research studies [17].

In the presence of wind, as illustrated in Fig. 2, the spherical shell with meshed net and the shell without a meshed net will experience significant vibration. It will also affect the flight performance of drones by adding meshed net aeroelasticity, the combination of wind load, and the material structure [18], [19]. Moreover, lightweight structures are sensitive to the wind load [20], [21], [22]. Thus, investigation of shelled drone's vibration response at different wind speeds to investigate each response.

Shelled drone eliminates the risk for a person to inspect a damaged infrastructure against safety and environmental hazards and prevents accidents if the shelled drone collides or needs to recover when stuck. The additional meshed net of the shelled drone will further augment the safety and survivability of the drone. This study assesses the shelled drone with added meshed net for bridge inspections and investigates how the aerodynamic performance [23] and vibration affect the drone stability. Consequently, the design provides the characteristics of the shelled drone to utilize for a specific inspection or purpose.

II. Related Works

Mizutani et al. (2014) investigated a quadrotor protected by a geodesic dome type's passive rotating spherical shell (PRSS) . The shell can rotate freely, enclosing the quadrotor with a gimbal frame so it can carry the impact of a collision. The passive rotating spherical shell can fly on narrow or complex spaces and is used for disaster response operation and infrastructure inspection, as shown in Fig. 3 [14]. The design is based on the relationship between the dome parameters and the radius of the circumscribed sphere along the selection of spherical shell structure, considering several parameters such as weight, strength, and maintainability. Furthermore, the designs' capabilities are tested by imposing the shell structure with à considerable number of simulated tests. The reason is that it is fabricated to apply it for bridge inspection while considering disaster response applications.

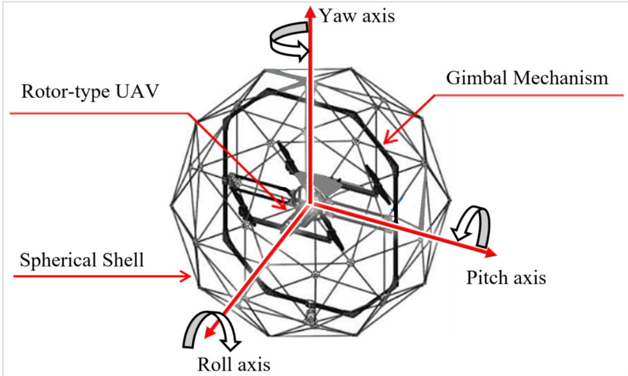

Fig. 3. Drone with passive rotating spherical shell

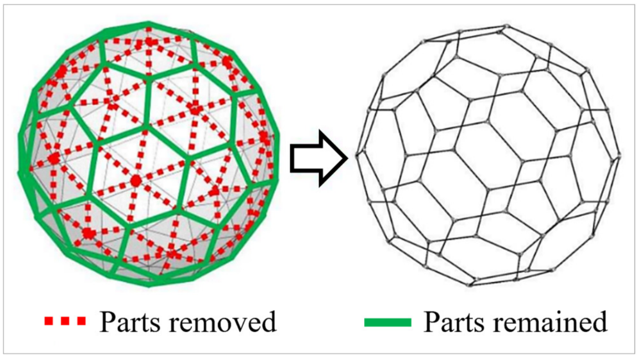

Fig. 4. Transformation of 3V geodesic to fullerene-type spherical shell structure

Per previous related studies, Salaan et al. (2015) conducted a design strategy for the passive rotating spherical shell drone. The design strategy includes the selection of the base drone, the spherical shell design and diameter, the gimbal structure, and the choice of materials. The design was verified through impact strength. Redesigning and reconfiguring some parts of the shell structure, considering the total number of joints and connections contributing to the overall weight of the PRSS, the 3V geodesic dome transformed into a fullerene type by removing some parts of the 3V geodesic dome [16], as shown in Fig. 4.

Salaan et al. [13] further investigated and developed the shelled drone on actual bridge conditions and requirements, as shown in Fig. 5. Simulation and actual bridge inspections verified its performance in acquiring images on different parts of the bridge without any fear of collision. The PRSS successfully demonstrated its abilities for the entire test, such as passing through limited space movement or rolling in contact with smooth and uneven surfaces.

Librado et al. developed the concept of adding meshed net for the shell through meshing and insulating strategies implementation for proximal visual inspection of distribution lines , as shown in Fig. 5 [17].

The shelled drone with meshed net used for distribution line proximal inspection illustrated the design profile in Fig. 6 [17]. The design concept of the study was based on the works of Mizutani, et al. [14] and Salaan, et al. [13]. With its meshing and insulation strategies, the spherical shell offers improved resiliency. The shell with meshed net prevented the

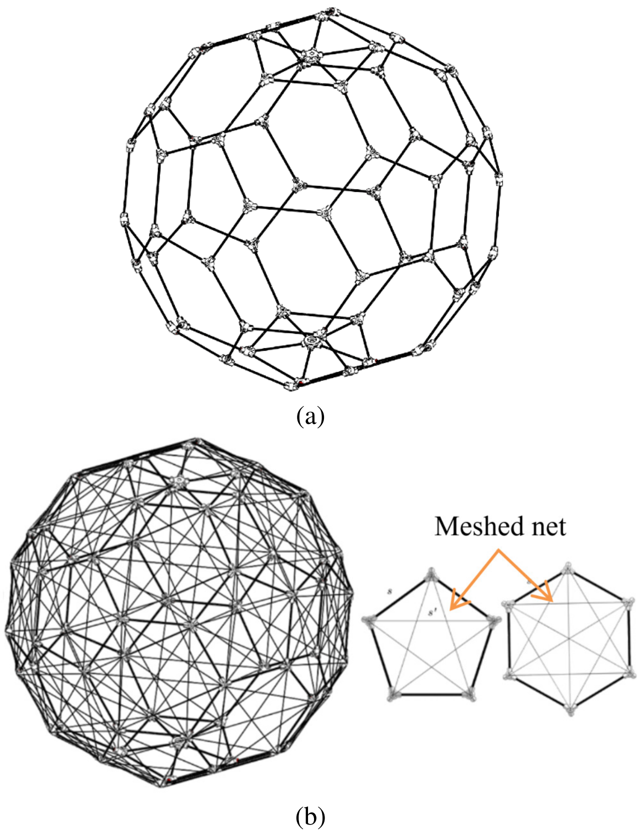

Fig. 5. Spherical shell without meshed net (a) and spherical shell with meshed net (b) from Librado et al. (2022)

Fig. 6. Close proximal visual inspection of distribution lines using shelled drone with meshed net from Librado et al. (2022)

intrusion of relatively smaller objects in the actual test.

III. Aerodynamic Evaluation Setup

The CFD simulation is an excellent method for analyzing a system's aerodynamic performance [24], [25]. Computational Fluid Dynamics (CFD) simulation was conducted as the first approach to assess the aerodynamic performance of the shelled-drone with meshed net and shelled-drone without meshed net through drag and lift force simulation data gathered. This procedure involved a series of simulations and a wind tunnel test to verify the aerodynamic performance. Specifications were initially designed for spherical shell weight, materials, shape, size, connections, joints, and meshed net material. The spherical shell was modeled and simulated through flow simulation.

A. Spherical Shell Preparation

1) Considerations for the Analysis of Shell Structure: The spherical shell design was based on the previous studies by Salaan et al. [16] since the fullerene-type spherical shell has less overall weight, reduced drag, and improved flight performance. The shell diameter dimension was based on the available wind tunnel size of 1200 mm x 845 mm test section. Also, the spherical shell size selection considered the blockage ratio requirement for wind tunnel testing [26].

2) Selection of Spherical Shell Specifications: As suggested in previous studies, the spherical shell joints and connections were made with aerodynamically efficient geometry and from appropriate lightweight but high-strength materials. The joints utilized an airfoil-type joint made of ABS plastic material. Moreover, lightweight carbon-fiber-reinforced plastic (CFRP) material was used for the connections. The system's robustness greatly relies on the spherical shell structure. Since the camera must have less obstruction from the spherical shell, thin connecting carbon rods showed great strength compared to carbon pipes during the impact test.

3) Selection of Meshed Net Material: The added meshed net was based on the recent work of Librado et al. [17]. The added meshed net to the fullerene-type shell's spherical shell was considered to augment further the drone's safety and survivability with the spherical shell. The material for the meshed net must also be lightweight, high strength, and can be easily installed. Polyamide, such as ordinary nylon, is an inexpensive, synthetic, fibrous material known for its high tensile strength, abrasion resistance, and chemical stability [27]. Polyethylene, such as fishing lines that are braided for additional strength, costs more than ordinary nylon; however, the more strands that appear in a weave of braided fishing line, the rounder and smoother it becomes; thus, the line has less friction, more resistant to abrasion, more durable and by weight, polyethylene strands are five to ten times sturdier than steel [28].

B. Theoretical Analysis

The drag force acts in a direction opposite to the relative flow velocity and depends on the shape and orientation of a body. The drag force can be calculated as [29]

$$F_d = C_d(A)(q) = C_d(A)(\rho)(v^2)/2$$

where dynamic pressure (q) is equivalent to $V^2/2$, A is the projected area of the body in the flow direction, Cd is the drag coefficient, and and v are air density and flow velocity, respectively.

C. Modeling and Simulation

The specifications and material should be initially designed to model the spherical shell with and without a meshed net in Computer-aided Design (CAD) software for selecting a spherical shell and meshed net. Then each model would be simulated using flow simulation. Flow simulation enables concurrent engineering and brings the critical impact of fluid flow analysis to ensure the proposed design will perform optimally. Before conducting the CFD simulation, the computational domain of the model must be defined [30].

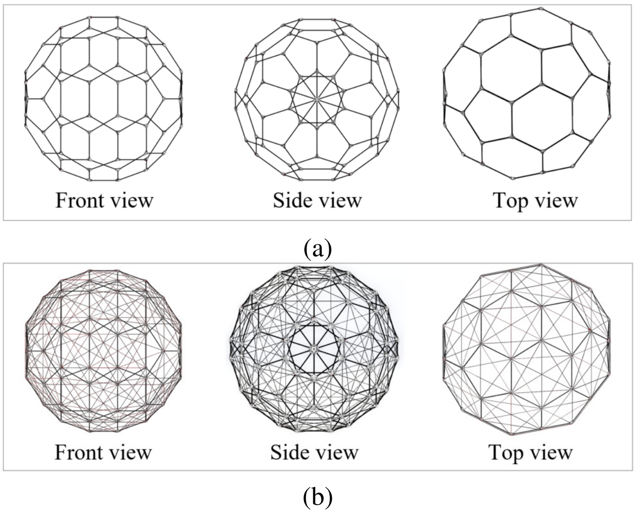

Fig. 7. CAD models of the spherical shell without a meshed net (a) and with meshed net (b)

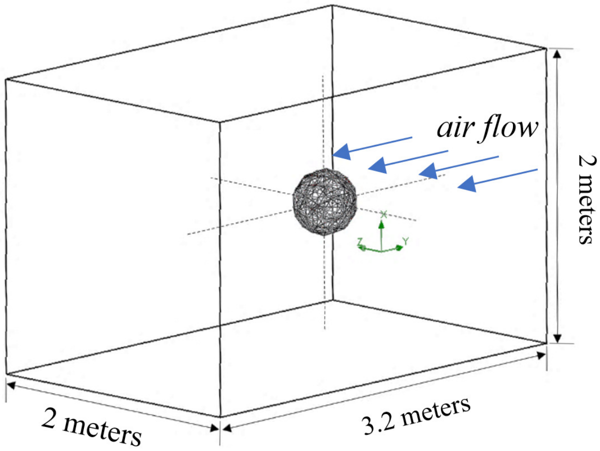

Fig. 8. The computational domain based on the recommended setting for choosing the domain for the CFD simulation requirement

1) CAD Model of Various Spherical Shells: As implemented in previous studies, CFD simulation is an excellent tool for analyzing the aerodynamic performance of a model. Fig. 7 illustrates the CAD designs for the various shells.

2) Setting the Computational Domain: From the upstream flow of the model, the recommended fluid domain should have a minimum of two (2) times the length of the model. This dimension should be enough to allow the flow to adjust due to the presence of the geometry. Generally, for the downstream flow, the model will shed a wake of lower energy flow. Thus, it is recommended to have a length minimum of five (5) times the dimension of the model along the direction of the flow to allow enough space for the boundary condition. A space of about two (2) times the model width on each side is also provided to allow for local flow deviation [31].

3) Flow Simulation Settings: In this procedure, the flow direction is parallel to the longitudinal axis of the shell, as shown in Fig. 9. Air temperature must be the ambient temperature in Iligan City, and the surrounding humidity should also be measured. Fine meshing and advanced channel refinement are necessary to get the simulation results accurately [32].

4) Parameters for the Flow Simulation: Design parameters for aerodynamic evaluation of the spherical shell with

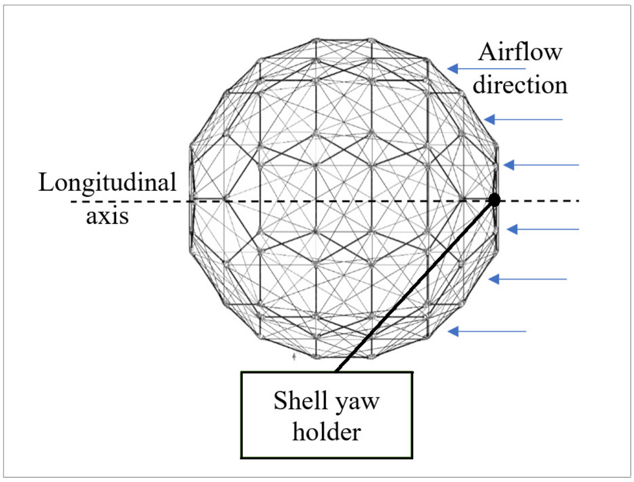

Fig. 9. The flow simulation setting showing the orientation of the spherical shell relative to the direction of the airflow

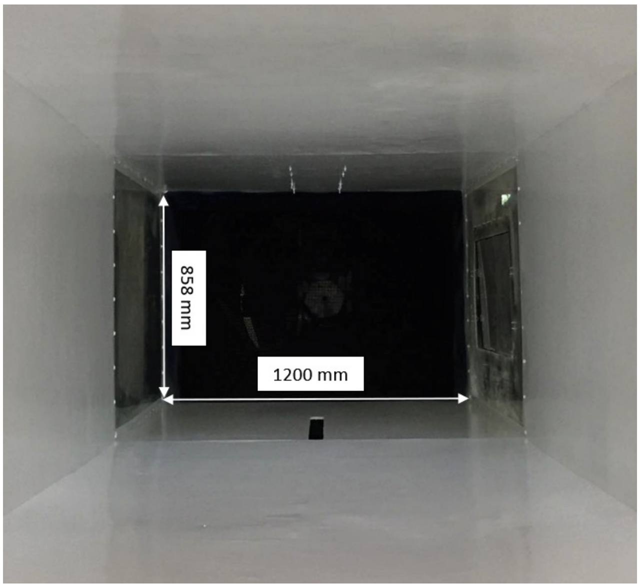

Fig. 10. Actual wind tunnel test section available with 1200-mm by 858-mm cross-sectional area

and without meshed net were based on the average wind speeds in Iligan City. The maximum value of the wind speed to use is the wind tunnel experiment maximum velocity for accuracy validation of the CFD simulation results.

D. Wind Tunnel Experiment

The available wind tunnel has a 1200mm x 845mm test section, a test range of 1 to 9 m/s, and an open loop tunnel with a real environment scenario, as shown in Fig. 10.

1) Wind Tunnel Preparation: The Wind Tunnel test section is made of acrylic material, and the diffuser is made of metal sheets for its base part and plywood for its inner part. The diffuser walls of the wind tunnel should be plain and smooth, so this part of the wind tunnel must be prepared. Moreover, the test section must be enclosed appropriately, ensuring that no air will escape through the chamber.

2) Velocity Profile Setup: Before the test, it is necessary to visualize first the velocity profile in the wind tunnel test section to insert the model properly inside. The model's position should be fixed inside because, in this manner

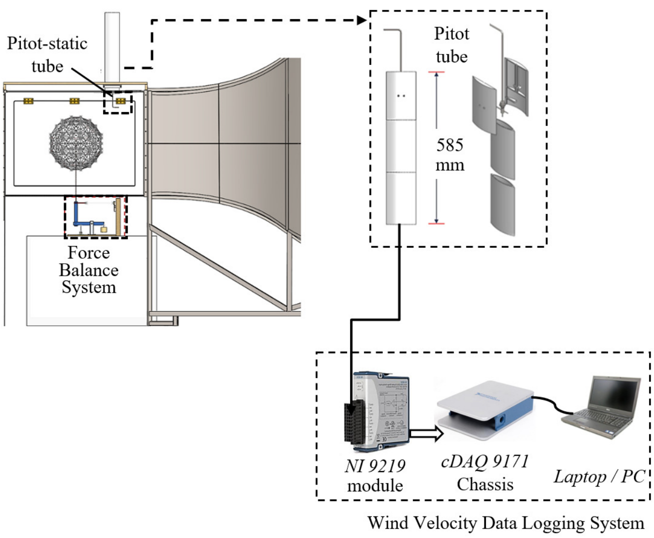

Fig. 11. Data acquisition system for velocity profile and velocity data gathering in wind tunnel testing

of velocity profile visualization, it will specify the correct conditions for the wind tunnel experiments. Furthermore, a velocity profile measuring system is suggested to be used to configure the proper position of the model.

The designed velocity profile measuring system using a pitot-static tube should be enclosed by an airfoil-shaped cover so that it will not obstruct the fluid flow in the test section when the pitot-static tube is inserted to measure the velocity at different points. The initial position of the measurement system was at the center of the test section. A fairing part was added when the airfoil-shaped cover was installed. This fairing effect reduces the drag and gives steady fluid flow caused by the in-between part of the cover and the outer part of the pitot-static tube. The fairing part was limited to the upper part of the test section, so the fluid flow visualization included the model and some of its surroundings.

The wind tunnel was prepared for velocity profile measurement using the pitot-static tube and its data logging system in Fig. 11. The data logging system consists of NI 9219 module and cDAQ 9171 chassis.

3) Blockage Ratio Measurement: Air flowing through the nozzle into the test section possesses a specific velocity profile. The blockage ratio is the ratio of the frontal or projected area of the model (A,model) over the cross-section area of the test section (A,test section). Based on the conducted wind tunnel experiments, a blockage of generally less than 5% should be preferred [33].

$$BlockageRatio = A_{model}/A_{testsection}$$

4) Design of Force Balance System: The force-balance system should be in static equilibrium with the model before conducting the wind tunnel experiment. The system should consist of the drag force measurement system. Furthermore, the materials used must be strong and withstand applied loads. Fig. 12 shows the design of the force balance system design considering the available wind tunnel test section dimension. The specifications and selections of the components focused on providing a strong foundation.

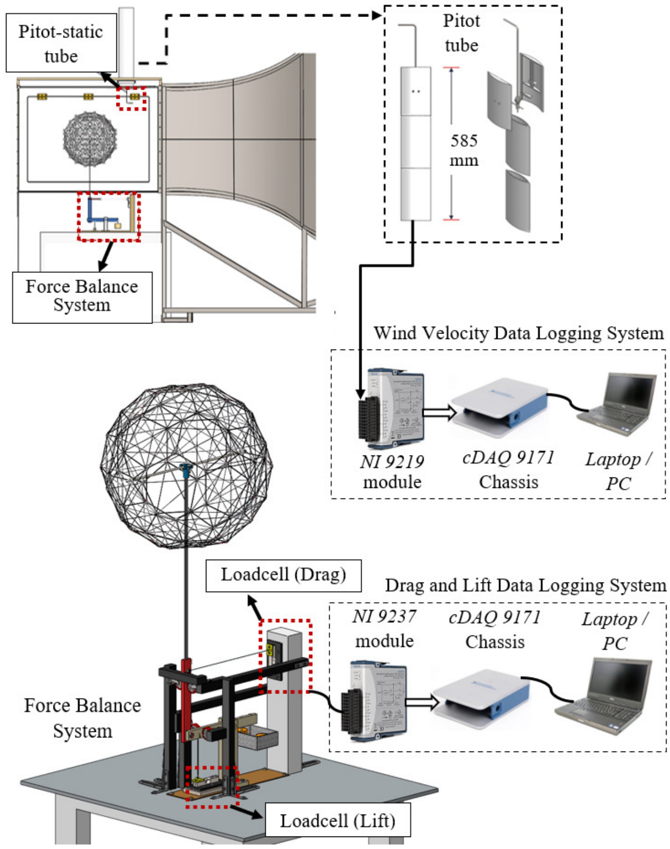

Fig. 12. Force-Balance System (FBS) and data acquisition system for wind tunnel test data gathering

5) Drag and Lift Force Interpretation: The data recorded from the drag and lift loadcell are not the drag and lift forces experienced by the spherical shell with meshed net and the shell without a meshed net. The drag and lift forces of the spherical shell were calculated through their respective moment arm values.

6) Data Acquisition System: The wind tunnel test results and the simulated aerodynamic results are used for verifying the gathered data. The data acquisition system for measuring wind speed and drag is illustrated in Fig. 12.

Through initial drag and lift force analysis simulation, the loadcell capacity was 1 kilogram, considering the available digital loadcells in the market. Two digital load cells were used, and all load application was in tension. The design was 3D-printed and used ABS plastic material. The lightweight string was attached from the linkages of the FBS and the load cell through this added 3D-printed part. The spherical shells were fabricated in the wind tunnel test, and the wind tunnel was prepared for velocity profile measurement using the pitot-static tube.

The data acquisition system for the wind tunnel test for aerodynamic analysis started from obtaining the velocity profile to gathering drag and lift force results. The velocity profile data logging system consists of NI 9219 module and cDAQ 9171 chassis. The NI 9219 module measured the signals from the pitot sensor. The drag and lift force data logging system consists of the TAL220B digital loadcells, NI 9237 module, and cDAQ 9171 chassis. And the digital loadcells were installed as shown in Fig. 13. The digital loadcells experiences tension load during the actual test.

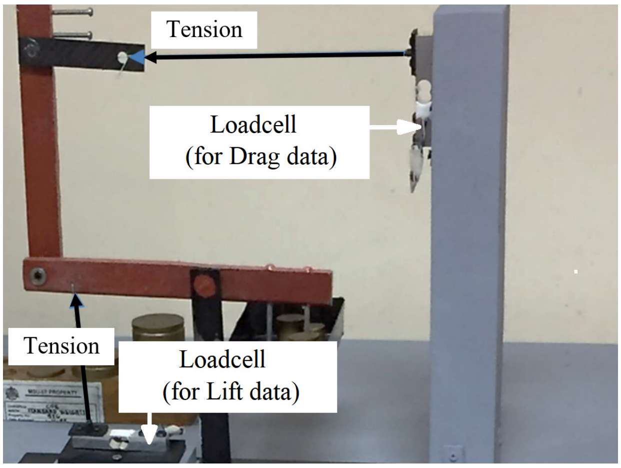

Fig. 13. Drag and lift loadcells used that are attached in the Force-Balance System

IV. Vibration Test Setup

The vibration response of the fullerene-type spherical shell with and without a meshed net was investigated at different wind speeds. Two types of meshed nets were used for comparative analysis. Through wind tunnel tests, frequency-response data at different wind speeds were extracted and analyzed in the MATLAB vibration toolbox.

A. Theoretical Analysis

The mechanical properties of a spherical shell with and without meshed nets of different materials vibrate differently. Considering the design or model vibration parameters, one can characterize each type of shell used and which performs better and best in this study. The vibration parameter, stiffness (k), viscous damping (c), damping ratio, and natural frequency are calculated as [34]:

$$w_n = \sqrt{k/m}$$

Vibration parameters such as k and c were usually measured through experiments, including drop testing, materials with high dynamic flexural modulus or stiffness exhibit low damping capacity and vice versa [35]. Frequency analysis also provides valuable information about structural vibrations.

TThe wind-induced response characteristics can be investigated and achieved between the frequency domain analytical model and actual tests concerning the magnitude and distribution of the monitored responses [36]. Thus, the vibration response of the spherical shell with and without the meshed net was investigated at different wind speeds. Fourier Transform is the most common mathematical technique for transforming time signals into the frequency domain [37].

B. Vibration Experimental Setup

In this procedure, to evaluate the vibration response of spherical shells with or without meshed nets of different materials, an actual vibration test had to be performed. In this study, two parts of the vibration test were made, data gathered focusing on the whole shell vibration and data collected on some parts of shell vibration. The wind tunnel test vibration set-up design is illustrated in Fig. 14 and Fig. 15. The vibration data could be measured using electronic sensors that convert vibration motions into electrical signals. This study used an accelerometer to gather the data at different wind speeds.

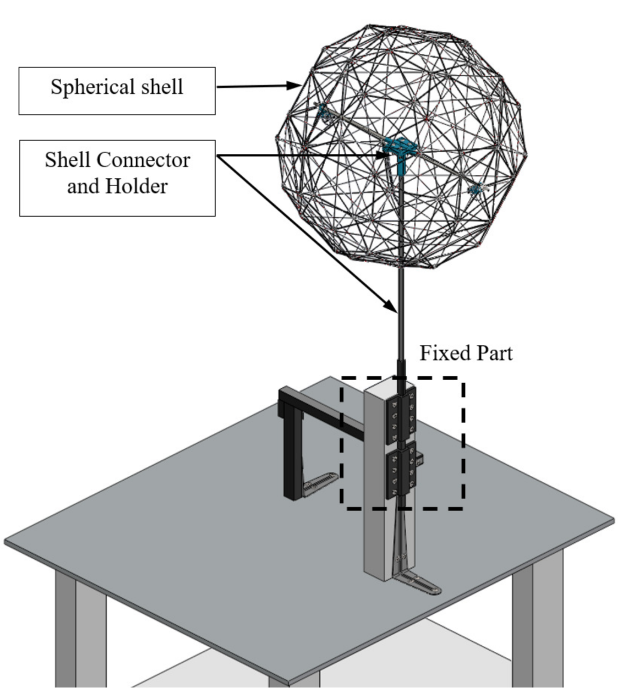

Fig. 14. Spherical shell connected with the shell connector and holder having the connector part fixed with the base for vibration wind tunnel test

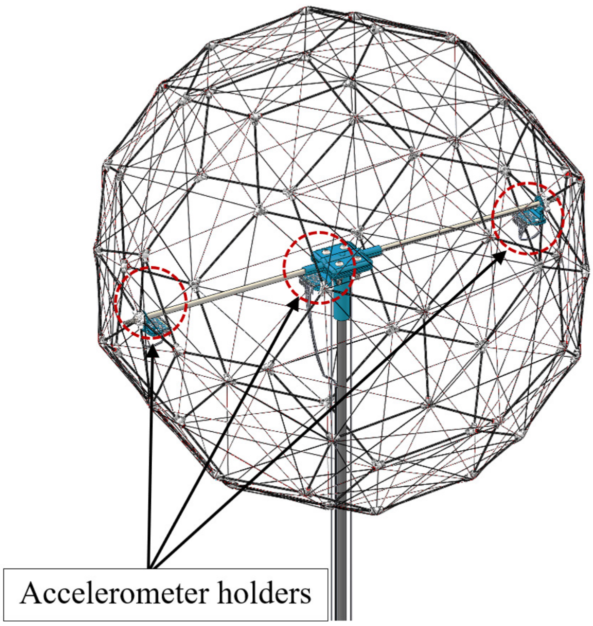

Fig. 15. Three accelerometer holders positioned at the center and the yaw holders of the spherical shell for vibration testing

C. Data Acquisition System for Vibration Experiment

The vibration data in the wind tunnel test was gathered through accelerometers, as shown in Fig. 18. The BNO055 9-degrees of freedom absolute orientation IMU (Inertial Measurement Unit) fusion breakout sensor was used in gathering the acceleration signal. The BNO055 is 9 degrees of freedom

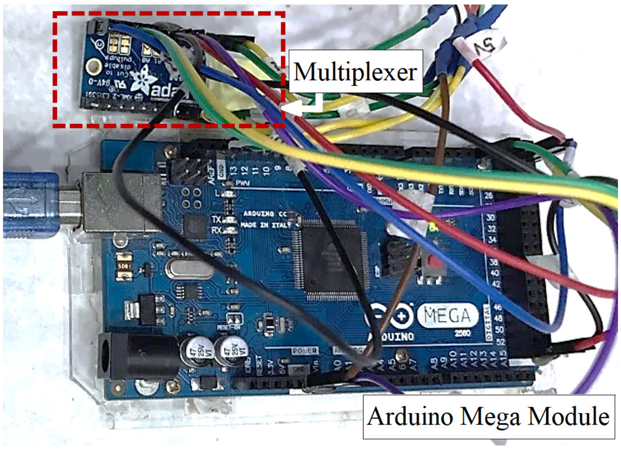

Fig. 16. The BNO055 sensor connected to the multiplexer for two or more connections sensor connection

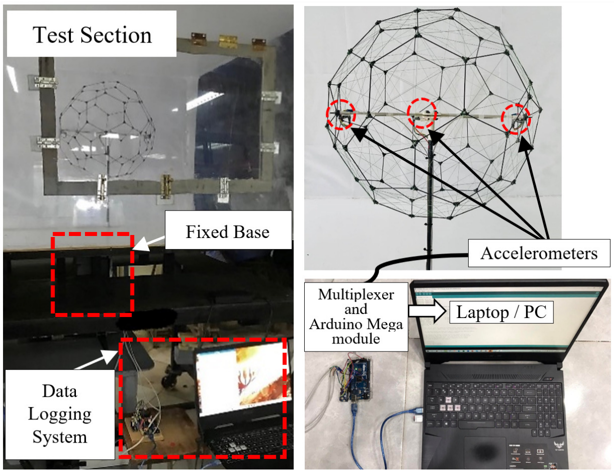

Fig. 17. Vibration data gathering wind tunnel test acquisition set-up

absolute orientation that blends accelerometer, magnetometer, and gyroscope data into stable three-axis orientation output by Bosch. This includes internal algorithms to constantly calibrate the gyroscope, accelerometer, and magnetometer inside the device connected through its vibration sensor module, as shown in Fig. 16. Implementation of vibration code was then set to one axis only that is parallel to the wind flow. Three accelerometers were used to evaluate further the vibration response of the whole spherical shell and some parts of the shell with or without a meshed net. The processed sensor signals then go to a multiplexer that selects the sensor to be digitized for two or more accelerometers.

Fig. 17 illustrates the experimental set-up for the vibration test in the wind tunnel, and the shell holder was fixed so that vibration of the shell would be evaluated only. The vibration base part was fixed during the wind tunnel test for vibration data gathering. In this study, two parts of vibration testing were made. First is using one accelerometer focusing on the center of the spherical shell, gathering the data at a higher sample rate than the first vibration test. The second part of the test uses three accelerometers connected to the multiplexer with its Arduino module to the laptop device for gathering the vibration data on the right and left sides of the shell. The data extracted in this case was derived along the direction of wind flow.

TABLE I
DESIGN PARAMETERS

Meshed Net Sizes	0.25 mm diameter 0.40 mm diameter 0.50 mm diameter
Wind Speed	2 m/s to 9 m/s
Sideslip Angles	0 degree 30 degrees 60 degrees

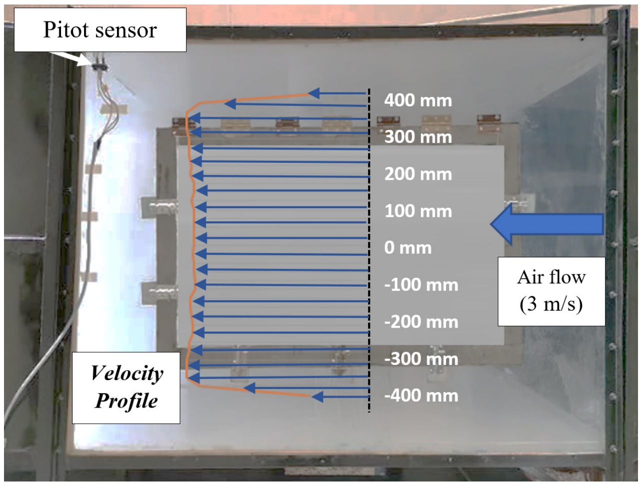

Fig. 18. Velocity profile of the wind tunnel test section from gathered wind tunnel test results

V. AERODYNAMIC RESULTS EVALUATION

The spherical shell design concept was a passive rotating spherical shell of fullerene-type structure based on previous related studies. In this study, a 400 mm diameter spherical shell with 1.5 mm diameter carbon rods was used, and the dimensions with an 800 mm shell of 3 mm carbon rods. This study could also assess the 800 mm shell through geometric similarity to the 400 mm shell. Flow simulation through Computational Fluid Dynamics (CFD) in SOLIDWORKS was conducted. A series of flow simulations were executed, and a wind tunnel test was performed.

The calculated blockage ratio indicated 3.48%, which satisfies the blockage ratio requirement for wind tunnel testing. Table 1 summarizes the design parameter. Evaluation of the aerodynamic performance of the shell with the meshed net was done for different sizes of the meshed net: 0.25 mm diameter net, 0.40 mm diameter net, and 0.50 mm diameter net.

Moreover, the added meshed net was evaluated using different materials for a 0.25 mm diameter meshed net. Monofilament nylon nets and multifilament (braided) fishing line nets were used to compare the aerodynamics of the spherical shell at different meshed net materials. Monofilament nylon is elastic and inexpensive in cost but can be easily broken or damaged. Meanwhile, braided fishing lines are more robust, non-stretchable, costly, and resistant to cuts or damages. These two types of the meshed net were compared and investigated.

In CFD simulation, the computational domain was set based on the standard dimensions of setting the domain. The

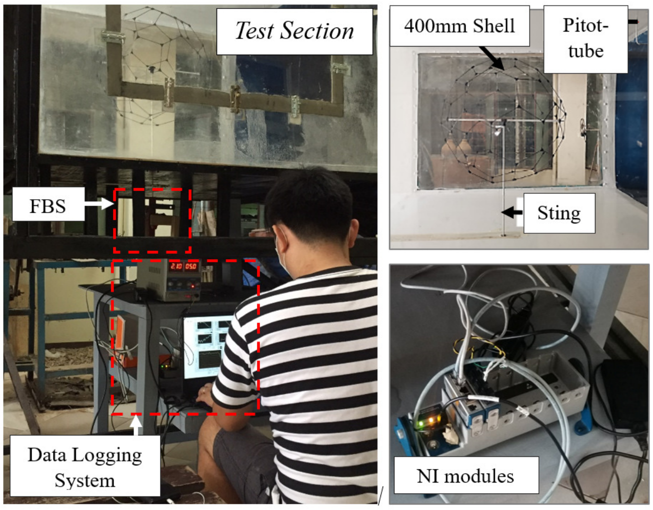

Fig. 19. Actual wind tunnel testing for aerodynamic results data gathering

computational domain is 2 x 2 x 3.2 meters. The ambient temperature and humidity were measured, having an average of 30° C and 69% values. The input velocities were set to 2, 4, 6, and 8 m/s, and the models were fine-meshed.

In wind tunnel testing, the spherical shells were fabricated, and the wind tunnel was prepared for velocity profile measurement using the pitot-static tube. Using the NI 9219 and cDAQ 9171 datasheet, the module with its chassis measured the pitot sensor's signals and converted them to digital data. The velocity data using NI LabView 2017 software was gathered and tabulated. With this test, the velocity profile of the wind tunnel's test section was visualized, as shown in Fig. 18. The force-balance system was initially designed and fabricated. The loadcells used were initially calibrated upon installation of the force-balance system under the wind tunnel test section. The force-balance system was adequately positioned and ensured static equilibrium at 0 m/s. The wind tunnel test results will validate the gathered simulated data using the SOLIDWORKS flow simulation.

Using the NI 9237 and cDAQ 9171 datasheet, the module with its chassis senses the signals from loadcell sensors and converts the analog signals to digitized data. The overall data acquisition system for aerodynamic analysis in wind tunnel test is illustrated in Fig. 19.

The simulated lift force results for spherical without a meshed net for 2 m/s to 8 m/s was about 0.0005 N to 0.002 N, respectively, which is almost zero. And the spherical shell with 0.25-mm meshed net lift forces was approximately 0.0006 N to 0.004 N. The wind tunnel test lift force data produced almost 0 N as well. It was concluded that the lift force experienced by the spherical shell with or without a meshed net is insignificant. Moreover, drones are made for hovering the whole assembly, including the spherical shell. Thus, the lift force does not significantly contribute to improving its performance.

To evaluate the aerodynamic performance of a spherical shell with meshed net, the CFD simulated model was validated by comparing the model results to the wind tunnel experimental data, as illustrated in Fig. 20. The lift force performance gave insignificant results. The drag force performance of the spherical shell gave significant results. Thus,

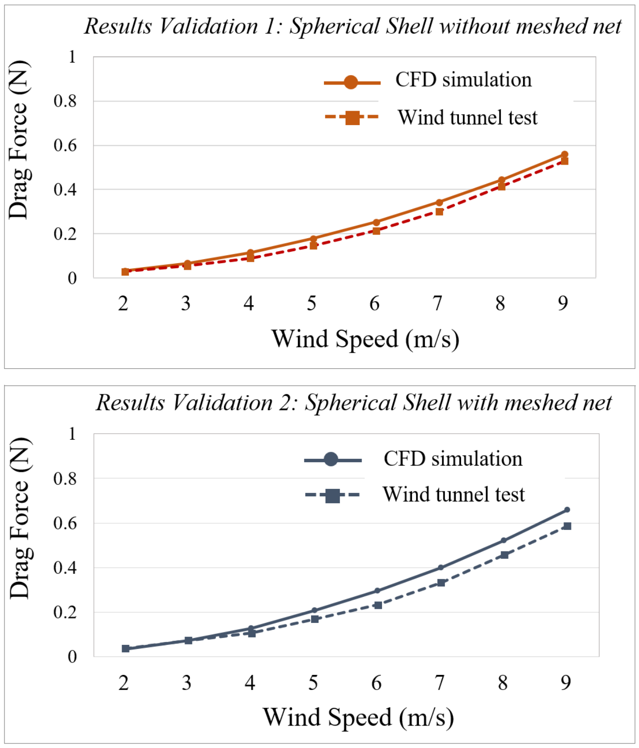

Fig. 20. Aerodynamic results validation for spherical shell without a meshed net and spherical shell with meshed net

the drag force data from the simulation and wind tunnel test was evaluated. The spherical shell with meshed net used for validation is the shell with monofilament nylon meshed net material. The simulated drag forces at 2 m/s to 9 m/s were compared with the wind tunnel data. The calculated percentage error of simulated drag force versus wind tunnel drag force for the spherical shell without a meshed net has an average value of 13.63%. The percentage error for a spherical shell with meshed net average value is 13.27%.

VI. Vibration Response Evaluation

In this study, two parts of vibration data gathering were made. The base part of the vibration test set-up was fixed during the wind tunnel experiment. First is the vibration response evaluation using one accelerometer focusing on the center of symmetry data of the spherical shell. The data gathered were at a higher sample rate than the second vibration test. The second part is the nodal vibration response evaluation using three accelerometers connected to the multiplexer with its Arduino module to the laptop device for gathering the vibration data on specific nodes on the shell.

Vibration test 1 focused on the center of symmetry data of the spherical shell, which is also the response of the whole spherical shell. The sample rate was set to 100 Hz (samples per second) for one accelerometer sensor only, at the center part in line with the shell holder to the fixed base part of the vibration test set-up.

Vibration test 2 used three accelerometers attached at specific points of the shell. The data extracted are derived along the direction of wind flow as shown in Fig. 21. Node 1 was located at the right-side frontal part of the shell, node 2 at the center part of the shell, and node 3 at the left-side end part of the shell as shown in Fig. 22. The sample rate

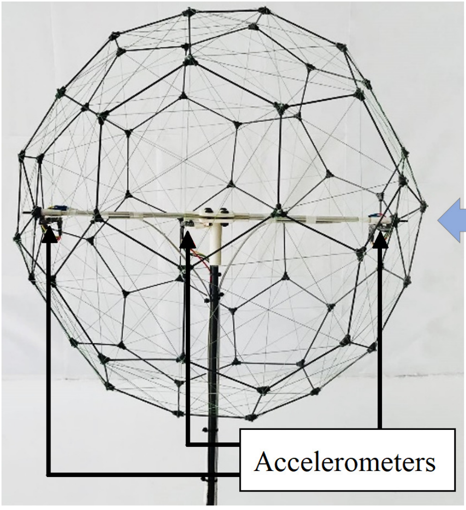

Fig. 21. Vibration test set-up through wind tunnel experiment of the spherical shell, three accelerometers were used and attached at specified nodes of the shell

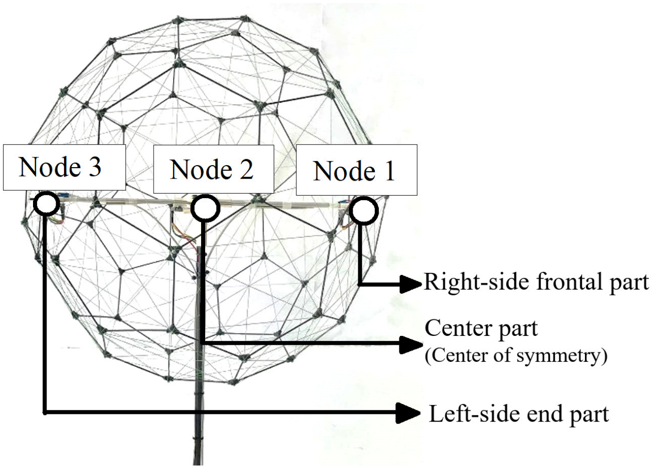

Fig. 22. Nodal analysis for the spherical shell response with airflow direction from the right, node 1 located at the right-side frontal part of the shell, node 2 located at the center part of the shell, and node 3 located at the left-side end part of the shell

was set to 33 Hz for each accelerometer sensor since it was set to 100 Hz for all sensors alternating from node 1 to node 2 to node 3. The vibration data at these points were gathered and tabulated for spherical shells without a meshed net, with 0.25 mm monofilament nylon and 0.25 mm braided fishing line.

Using the MATLAB vibration toolbox by Tom Irvine, the gathered time-domain vibration response data were converted to frequency-domain response through Fourier Transform. Fourier Transform is a method for representing a time history signal in terms of a frequency domain function. This software applied a Hanning window for stationary vibration for time-domain data signal analysis. It is because the rectangular window produces more leakage errors [33].

The vibration response was investigated for the spherical shell without a meshed net, with a monofilament nylon net, and with a braided fishing line meshed net. Gathered data for different wind speeds up to four tests were extracted for further analysis.

The stability of the shell drone without a meshed net and the shell drone with the meshed net can also be determined

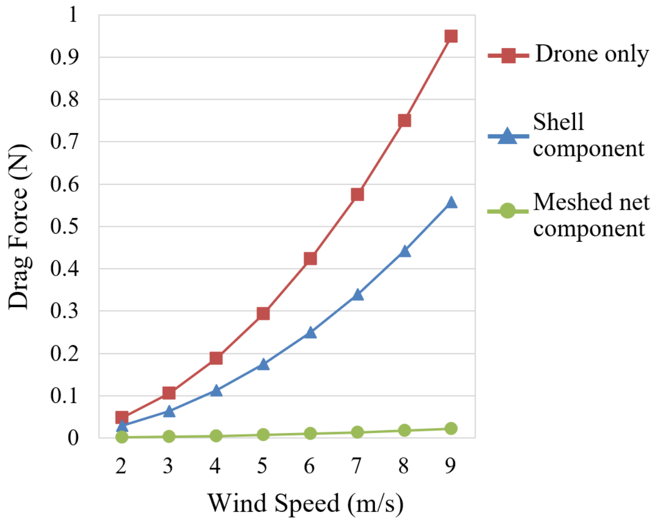

Fig. 23. Drag force comparison for shelled drone components (drone, shell component, and the added meshed net component)

using the resulting damping effect of the system. The compiled program from the MATLAB vibration toolbox by Tom Irvine was used to carry out the vibration frequency response corresponding to various values of the natural frequency and damping factor. Thus, the half-power bandwidth method or technique performs a curve-fit to determine the damping ratio for the spherical shell with a meshed net system excited by an airflow force due to airflow pressure. The compiled program from the MATLAB vibration toolbox includes the damping effect provided several trials for the curve-fitting and the margin frequency based on the generated frequency-response results.

VII. Results and Discussion

A. Aerodynamic Results

The simulated model of the shell with and without meshed net using CFD (Computational Fluid Dynamics) was validated by comparing its results to the wind tunnel experimental data to evaluate the aerodynamic performance of a spherical shell with the meshed net. The simulated drag forces at 9 m/s are 0.56 N and 0.66 N, while the wind tunnel data are 0.53 N and 0.59 N for fullerene-type shells without a net and meshed net, respectively. The percentage error of simulated drag force versus wind tunnel drag force for the two spherical shells was computed to be 5.67% and 10.889%, respectively.

The shelled drone consists of the drone, attached shell, and gimbal. Fig. 23 shows the drag force differences of the drone, with its added shell and the meshed net of 0.25mm in size. At 9 m/s, the drone alone has a more significant drag experienced by 0.95 N. With its added shell, the drag contribution of 0.56 N gives the shelled drone an overall drag value of 1.51 N. Moreover, the added meshed net drag contribution is only 0.022 N, which offers an overall drag value of 1.53 N for a shelled drone with added meshed net at this specific wind speed. The added meshed net gives an average value of 1.52% drag contribution for the shelled drone.

Flow visualizations are generated to illustrate the characteristics of the flow of air to the shell with meshed net and the

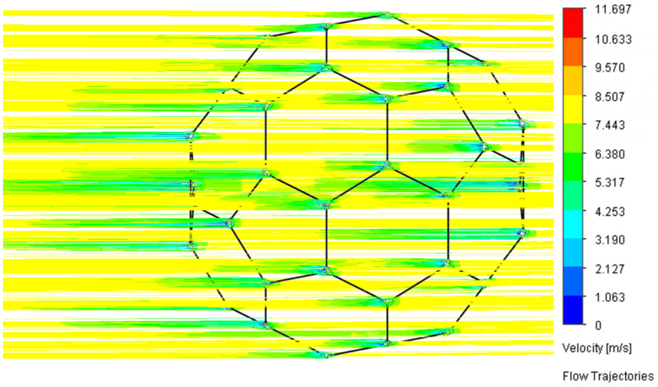

(a)

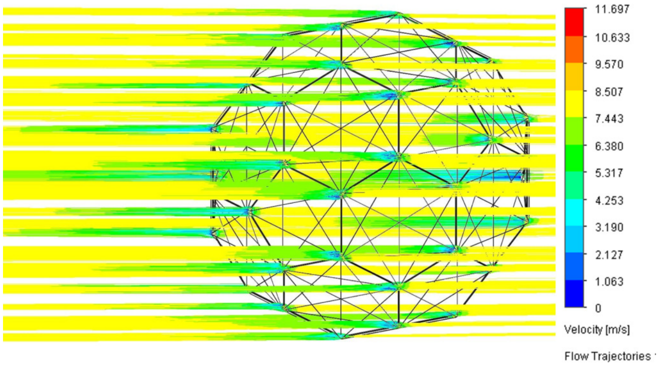

(b)

Fig. 24. Flow visualization of fullerene-type structure spherical shell (a) and spherical shell with meshed net (b) showing wake regions at airfoil joints

TABLE II
INCREASE IN DRAG FOR SHELLED DRONES DUE TO DIFFERENT MESHED NET SIZES

Wind Velocity (m/s)	0.25 mm meshed net	0.40 mm meshed net	0.50 mm meshed net
2	1.68 %	2.45 %	5.94 %
4	1.54 %	2.13 %	5.41 %
6	1.49 %	2.02 %	5.30 %
8	1.44 %	1.91 %	5.14 %
9	1.42 %	1.92 %	5.13 %

TABLE III
INCREASE IN DRAG FOR SHELLED DRONES DUE TO DIFFERENT MESHED NET MATERIAL USED

Wind Velocity (m/s)	with monofilament nylon meshed net	with braided fishing line meshed net
2	1.68 %	1.77 %
3	1.63 %	1.69 %
4	1.49 %	1.62 %
5	1.49 %	1.58 %
6	1.45 %	1.58 %
7	1.68 %	1.57 %
8	1.44 %	1.50 %
9	1.42 %	1.54 %

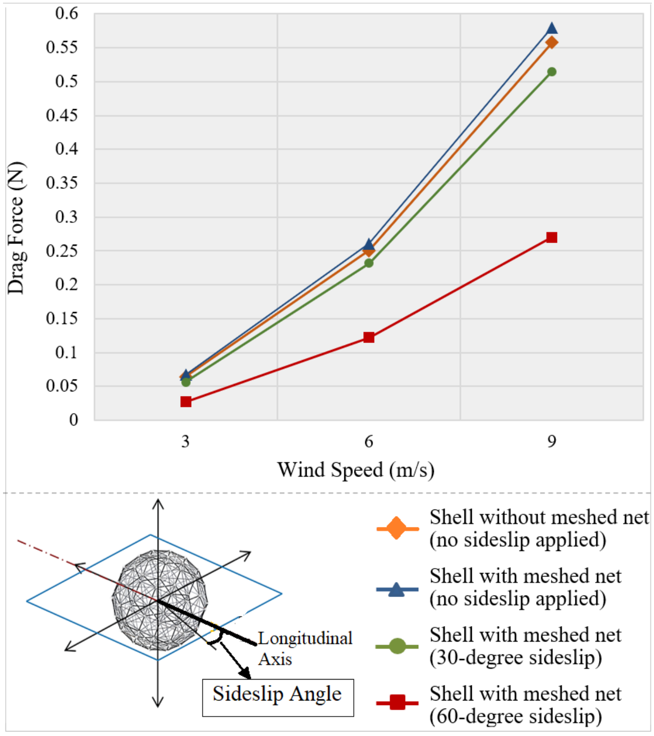

Fig. 25. Drag forces for spherical shells at different sideslip angle application

surface with a meshed net. And with this, the numerical and visual results of the simulation are presented. As shown in Fig. 24, the shell without a meshed net has lesser wake flow regions than the shell with the added meshed net; this is due to the added part of the meshed net, which has cylindrical geometry—the flow forms over the front and back of the cylinder. From the front yaw holder or the right side of the shell, the flow smoothly passes over the meshed net installed at the yaw holder. But in the wake, the flow is usually highly unsteady, and large vortices were found downstream, which gives wake-induced vibration. This study investigated the vibration response of the meshed net's shell with the meshed net, and the results are discussed in this section.

Considering the different meshed net sizes, as summarized in Table 2, the shelled drone with a 0.25 mm meshed net indicated an average of 1.52% increase in drag. There was a 2.10% increase in drag force for the shelled drone with a bigger net size of 0.40 mm, and a 5.37% increase for the shelled drone with a net size of 0.50 mm.

In consideration of the type of material for the meshed net, as summarized in Table 3, the shell with nylon meshed net, and the braided fishing line meshed net indicated almost the same drag force values. It is because drag force is proportional to the projected area, and these different meshed net materials modeled in SOLIDWORKS have the same geometry. However, when the gathered CFD results for drag force values are evaluated, the shell with braided fishing line meshed net indicated an increased drag of an average of 1.61% compared to the nylon meshed net having 1.52%. It is because of the material considered in modeling the spherical shells in the SOLIDWORKS program, where the braided fishing line meshed net has a surface roughness that contributes to the friction force opposite to the drag force.

Considering the application of different sideslip angles, as shown in Fig. 25, the drag force decreased by an average of 3.47% for the shelled drone with a monofilament nylon meshed net. In contrast, 2.43% shelled drone with braided fishing line meshed net at 30° sideslip angle application. At increasing sideslip angle, the drag force decreased by 18.7% at 60° sideslip angle for the shelled drones of any meshed net material. The projected area of the wind flow is from the face or side of the shell with the gimbal holder. Thus, to attain better performance during bridge inspection, the shell with meshed net yaw holder should be sideways to reduce the projected area.

B. Vibration Response Results

1) Vibration-Frequency Response Evaluation: The first vibration response evaluation focused on gathering vibration data of the center of the spherical shell at a higher sample rate than the second vibration test. Fig. 26 shows the generated vibration frequency response for the gathered vibration data of the whole spherical shell in the wind tunnel experiment. The sample rate was set to 100 Hz (100 samples per second) for one accelerometer sensor only, at the center part in line with the shell holder to the fixed base part of the vibration test set-up. At increasing velocities, the amplitude is higher for the spherical shell with a braided meshed net which makes the system behave poorly compared to the spherical shell with a monofilament nylon meshed net. It is because of the braided net's mechanical properties, which are non-stretchable compared to the monofilament nylon net.

2) Nodal Vibration-Frequency Response Evaluation: Since the spherical shell with the meshed net has a better vibration response, this study considered evaluating specific points on the shell for nodal vibration response evaluation. These points or nodes are located at the shell's right-side frontal part (node 1), the center part or center of symmetry data of the shell (node 2), and the shell's left-side end part (node 3). For gathering the vibration data at these points, the sample rate was set to 33 Hz (33 samples per second) for each accelerometer sensor, alternating from node 1 to node 2 to node 3. The vibration data at these points were gathered and tabulated for spherical shells without a meshed net, with 0.25 mm monofilament nylon and 0.25 mm braided fishing line.

For nodal vibration response evaluation, at nodes 1, 2, and 3, the spherical shell with monofilament nylon meshed net vibration response has a lesser amplitude value than the shell with braided fishing line meshed net at 4m/s velocities. As shown in Fig. 27, the amplitude value of the spherical shell with braided fishing line meshed net at node 1 at the right-side frontal part and node 3 at the left-side end part is 0.089 and 0.075, respectively. While the amplitude value of the spherical shell with monofilament nylon meshed net at nodes 1 and 3 is 0.071 and 0.07, respectively. With nodal vibration response evaluation of monofilament nylon meshed net, it was found that the frontal part (node 1) and end part (node 3) of the shell's vibration response tend to behave similarly because peak amplitude values are approximately equal.

3) Evaluation of Shell Stability : The shell system's stability was also determined using the system's damping factor or damping ratio. As shown in Fig. 28, the damping ratio for the shell without the meshed net and shell with different materials of meshed net indicated an equivalent damping ratio from 0 to 1, which implied that the system is underdamped. Based on the curve-fit graphs of frequency-response data of 10,000 iterations, the maximum damping ratio calculated was 0.4 for a shell without a meshed net and a shell with a meshed net of any material type (monofilament nylon or braided fishing line). Thus, the damping ratio is between 0 to 1, implying that the shell without a meshed net and the shell with a meshed net combination are under-damped systems, as further summarized in Table 4.

In addition, the frequency-response results from previous graphs also support the shell stability in which the resulting oscillations gradually decrease to zero as the system reaches

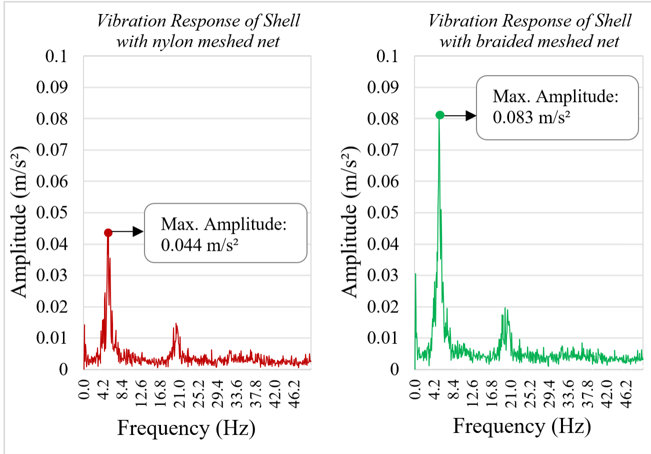

(a)

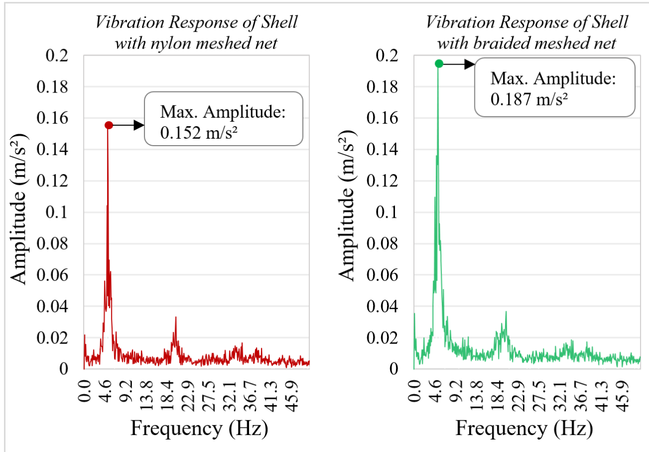

(b)

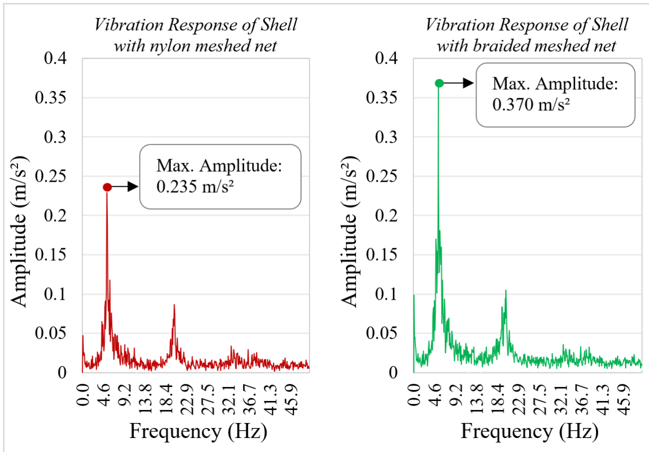

(c)

Fig. 26. Vibration frequency-response of the shell with different meshed net materials used in the wind tunnel test at 4 m/s air velocity (a), 6 m/s air velocity (b), and 8 m/s air velocity (c)

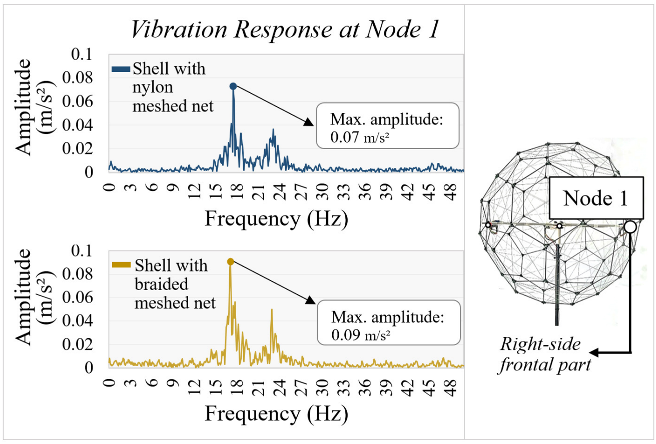

(a)

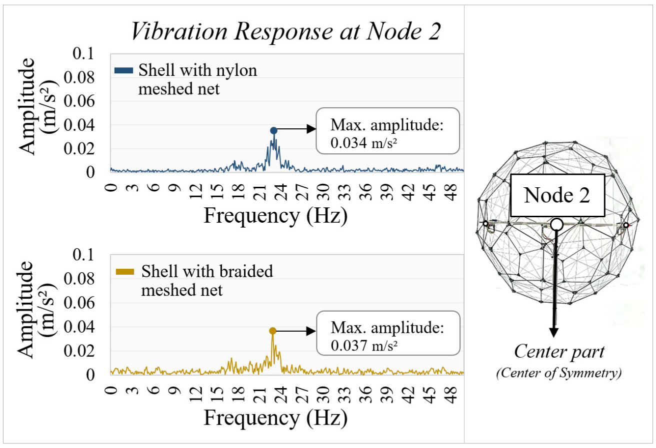

(b)

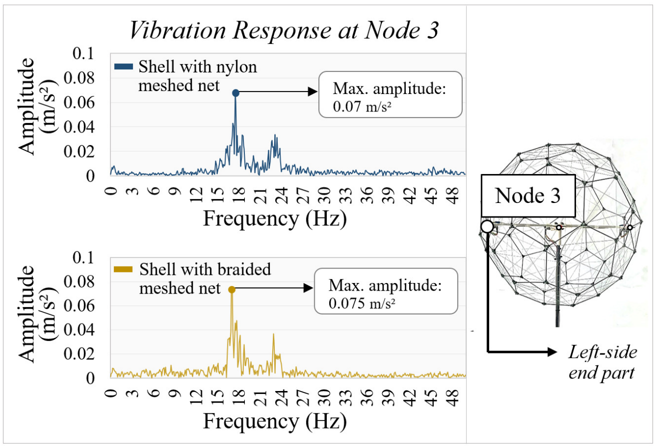

(c)

Fig. 27. Nodal vibration frequency-response of the shell with node 1 located on the right-side frontal part of the shell (a), node 2 on the center part of the shell (b), and node 3 on the left-side end part of the shell (c), for air velocity of 4 m/s

its steady state. The shell without a meshed net and the shell with a meshed net from its equilibrium position vibrates about the equilibrium point without exhibiting any secular trend; the system neither returns to the equilibrium nor moves away with it with time. Thus, the shell without a net and the shell with a meshed net of any material type showed system stability.

4) Verification of Shell-drone Stability : An actual bridge inspection was performed considering the presence of wind

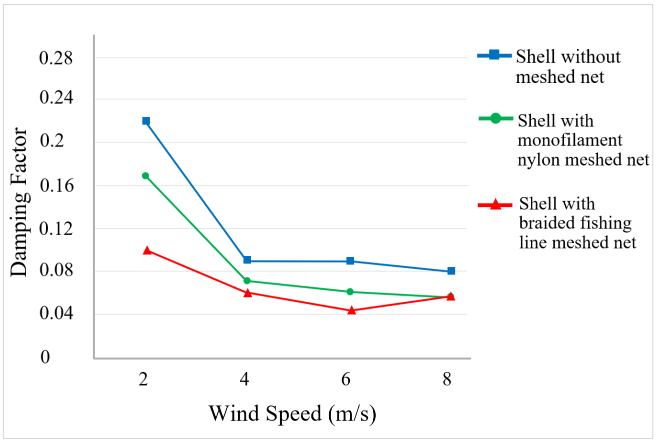

Fig. 28. Generated damping factor of spherical shells without meshed net and shell with different meshed net materials

TABLE IV
SHELL STABILITY THROUGH DAMPING EFFECT

	Maximum Damping Ratio	System Response
Shell without net	0.40	Underdamped, Stable
Shell with monofilament nylon meshed net	0.35	Underdamped Stable
Shell with braided fishing line meshed net	0.30	Underdamped, Stable

Fig. 29. Actual flight test using shelled drone with meshed net

on the bridge in Iligan City, Philippines, using the shelled drone with the monofilament nylon meshed net as shown in Fig. 29. During the flight test, wind gustiness was experienced, with a recorded maximum wind speed of 6 m/s. An onboard camera was installed to visually inspect the bridge girders for the actual flight test.

The shelled drone first inspected the outside part of the bridge girder with its first collision recorder, as shown in Fig. 30. After the inspection of the outside part of the girder, the shelled drone inspected the bridge girders, going inside the tubular flange where the second collision made as shown in Fig. 31.

Fig. 32 shows the gathered rotation data of the shelled

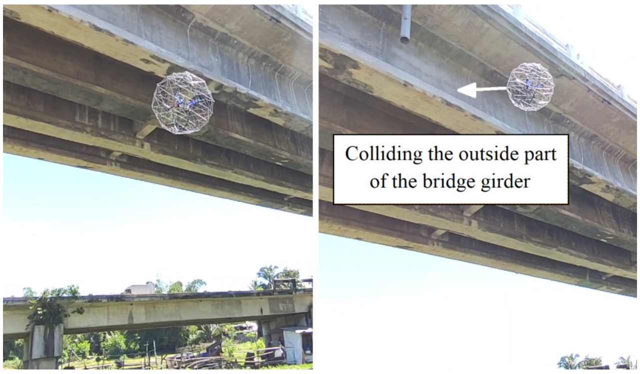

Fig. 30. Actual flight test of the shelled drone with meshed net colliding the outer part of the bridge girder (first collision)

Fig. 31. Actual flight test of the shelled drone with meshed net colliding the bridge girders (second collision)

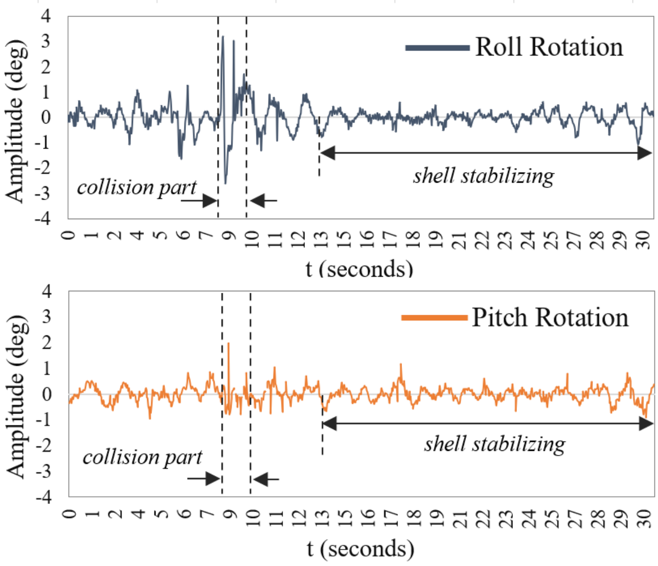

Fig. 32. The gathered rotation data in the event of the first collision and after the shelled drone collision with meshed net show the shell system's stability

drone in the event of the first collision of the outer part of the bridge girder. It was found that the shelled drone showed system stability after the collision. The resulting amplitude values for pitch and roll rotation of the shelled drone with meshed net gradually fall to the zero-degree pitch and roll rotation angle as the system reaches its steady state.

Moreover, the gathered rotation data during the second collision of the shelled drone going to the innermost part

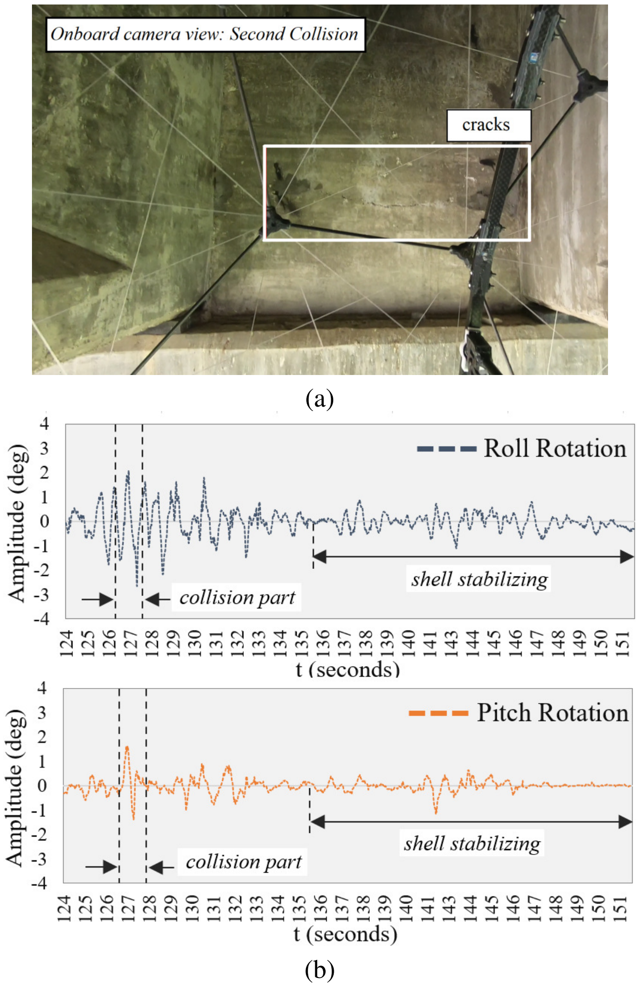

Fig. 33. The onboard camera view shows cracks of the bridge in the event of the second collision (a), and the gathered rotation data during the second collision (shelled drone going to the innermost part of the bridge girder) and after collision showing the shell system's stability (b)

of the bridge girder, as shown in Fig. 34, further supports the shell-drone with meshed net stability results from the first collision. One of the applications of the shelled drone with the meshed net is to inspect infrastructures efficiently and effectively through visual inspection. It can be observed how bridge cracks were found on the actual flight test of the bridge, as shown in the onboard camera view of Fig. 33.

Through the gathered bridge inspection data, the pitch and roll angles gave significant results for analyzing the stability of the shelled drone with the meshed net system. The collision of the shelled drone resulted in a change of the shell's rotation in roll angle of lesser than 3.2 degrees and a change in pitch angle of 2 degrees, as shown in Fig. 34 and Fig. 35, respectively. Moreover, the shelled drone became stable after the collision even with the wind's presence, with less than a 1-degree change of pitch and roll angles only.

With the actual bridge inspection results, the flight performance of the shelled drone with meshed net for stability consideration verified the vibration response results. monofilament nylon meshed has a better overall response. Furthermore, because the spherical shell with a braided fishing line meshed net has higher amplitude values, the shell will more likely experience deformation because of how high it moves from its initial position. Moreover, the effect of the elasticity of nylon material with the airflow makes its overall

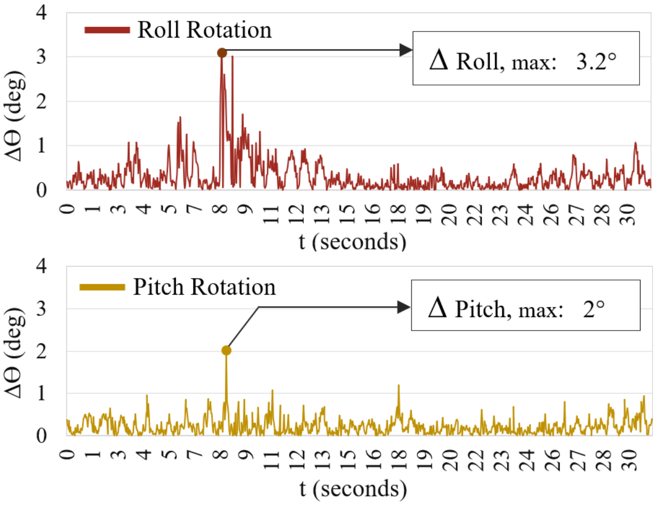

Fig. 34. Data representation of change in pitch and roll of the shelled drone with the meshed net in the event of the first collision

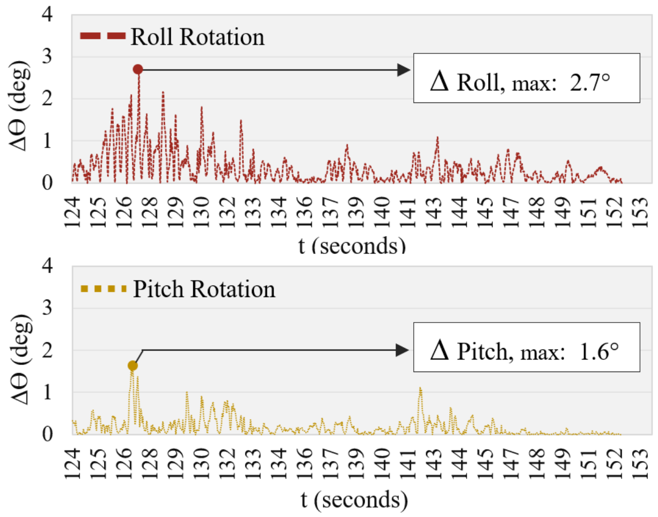

Fig. 35. Data representation of change in pitch and roll of the shelled drone with the meshed net in the event of the second collision

shell structure aeroelastic and has a better vibration response.

VIII. CONCLUSION

In this study, the shelled drone's aerodynamic performance and vibration response with meshed net are evaluated. The aerodynamic performance of the shelled drone was successfully implemented using flow simulation and wind tunnel experiment. The addition of meshed net increased the drag force of the shelled drone by 1.52% for the ordinary nylon material and 1.61% for the braided fishing line material. Thus, the added meshed net gives only an average value of 1.56% drag contribution for any meshed net material type for the shelled drone. The drag force decreased by an average of 2.95% at a 30° sideslip angle and 19% at a 60° sideslip angle for the shelled drone with any meshed net material.

Considering the vibration response of the shelled drone, the shell with braided fishing line meshed net indicated high amplitude values, from which it can be concluded that the system behaves poorly during inspections. In contrast, the shell with the monofilament nylon meshed net showed a better vibration response. The actual bridge inspection also verified the performance of the shelled drone with monofilament nylon meshed net, considering the system stability.

Generally, the shelled drone's aerodynamic performance and vibration response with monofilament nylon meshed net is better than the shell with braided fishing line meshed net. The 1.52% drag contribution is still a good trade-off for the safety and survivability of the drone, especially for bridge inspections.

REFERENCES

[1] Emanuele Adorni, Anastasiia Rozhok, Roberto Revetria, and Mikhail Ivanov, "Literature Review on Drones Used in the Surveillance Field," Lecture Notes in Engineering and Computer Science: Proceedings of The International MultiConference of Engineers and Computer Scientists 2021, 20-22 October, 2021, Hong Kong, pp178-183

[2] J. Seo, L. Doque and J.Wackerr, "Drone-enabled bridge inspection methodology and application," Automation in Construction, https://doi.org/10.1016/j.autcon.2018.06.006. 2018.

[3] A. Briod, J. C. Zufferey, P. Kornatowski, and D. Floreano, "A collision resilient flying robot," in 2014 Journal of Field Robotics (JFR), vol. 31, no. 4, pp. 496–509, November 2014.

[4] J. C Zufferey, A. Beyeler, and D. Floreano, "Vision-based control of near-obstacle flight," in 2009 Auton Robot, vol 27, pp. 201–219, 2009.

[5] J. Roberts, T. Stirling, J. C. Zufferey, and D. Floreano, "Quadrotor using minimal sensing for autonomous indoor flight," In European Micro Air Vehicle Conference and Flight Competition (EMAV2007) pp. 17–21, 2007.

[6] D. Schafroth, S. Bouabdallah, C. Bermes, and R. Siegwart, "From the test benches to the first prototype of the muFly micro helicopter," Journal of Intelligent and Robotic Systems, vol. 54, pp. 245–260, DOI: 10.1007/s10514-009-9139-6.

[7] A. Bachrach, R. He, and N. Roy, "Autonomous flight in unknown indoor environments," International Journal of Micro Air Vehicles, vol. 1(4), pp. 217–228, 2009.

[8] S. Shen, N. Michael, and V. Kumar, "Autonomous multirotor indoor navigation with a computationally constrained MAV," In Robotics and Automation (ICRA), 2011 IEEE International Conference, pp. 20–25, 2011.

[9] A. Kalantari and M. Spenko, "Design and experimental validation of that, a hybrid terrestrial and aerial quadrotor," in 2013 IEEE International Conference on Robotics and Automation, pp. 4430–4435, May 2013.

[10] K. Malandrakis, R. Dixon, A.Savvaris, and A. Tsourdos, "Design and development of a novel sphericalUAVv," in Proceedings of 20th IFAC Symposium on Automatic Control in Aerospace (ACA 2016), vol. 49, no. 17, pp. 320–325, 2016.

[11] C. J. Salaan, K. Tadakuma, Y. Okada, E. Takane, K. Ohno, and S. Tadokoro, "Uav with two passive rotating hemispherical shells for physical interaction and power tethering in a complex environment," in 2017 IEEE International Conference on Robotics and Automation (ICRA), July 2017.

[12] C. J. Salaan, K. Tadakuma, Y. Okada, Y. Sakai, and K. O. S. Tadokoro, "Development and experimental validation of aerial vehicle with a passive rotating shell on each rotor," in 2019 IEEE International Conference on Robotics and Automation (ICRA), vol. 4, pp. 2568 – 2575, July 2019.

[13] C. J. Salaan, Y. O.andd S. Mizutani, T. Ishii, K. Koura, K. Ohno, and S. Tadokoro, "Close visual bridge inspection using UAV with a passive rotating spherical shell," in Journal of Field of Robotics, vol. 35, pp. 850–867, February 2018.

[14] S. Mizutani, K. Ohno, K. Yanagimura, Y. Okada, E. Takeuchi, and S. Tadokoro, "Quadrotor with a Rotating Spherical Shell Which Can Fly in the Complex Structure," Robotics and Mechatronics Conference, 2014.

[15] S. Mizutani, Y. Okada, C. J. Salaan, T. Ishii, K. Ohno, and S. Tadokoro, "Proposal and experimental validation of a design strategy for UAV with a passive rotating spherical shell," in IEEE/RSJ International Conference on Intelligent Robots and Systems (IROS), pp. 1271–1278, December 2015.

[16] C. J. Salaan, Y. Okada, K. Hozumi, K. Ohno, and S. Tadokoro, "Improvement UAV's flight performance by reducing the drag force of spherical shell," in 2016 IEEE/RSJ International Conference on Intelligent Robots and Systems (IROS), December 2016.

[17] L. Librado, C. Cahig, C. A. Banglos, J. Pao, and C. J. Salaan, "Meshing and Insulation Strategies for Shelled UAVs in Proximal Inspection of Distribution Utility Lines," in 2022 IEEE Robotics and Automation Letters, March 2022.

[18] S. J. Ying, Advanced Dynamics, American Institute of Aeronautics and Astronautics, Inc. 1997.

[19] L. Meirovitch, Fundamentals of Vibration, McGraw-Hill, 2017

[20] Z. Zhang and Y. Tamura, ”Wind Tunnel Test and Wind-induced Vibration Analysis of Spherical Domes,” Advanced Steel Construction 2 (2006) 71-86, 2006.

[21] H. Huang, Y. Xian, W. Zhang, M. Guo, K. Yang, and K. Xi, ”Analysis of Wind-Induced Vibration of a Spoke-Wise Cable–Membrane Structure,” Journal of Marine Science and Engineering, August 2020.

[22] W. Lili, S. Yongjiu and W. Yuanqing, ”Wind-Induced Response Characteristics of Monolayer Cable Net,” Journal of Engineering Mechanics, DOI: 10.1061/ ASCE 0733-9399 2010 136:3 311, March 2010.

[23] Yalin Pan, Jun Huang, Feng Li, and Chuxiong Yan, ”Integrated Design Optimization of Aerodynamic and Stealthy Performance for Flying Wing Aircraft,” Lecture Notes in Engineering and Computer Science: Proceedings of The International MultiConference of Engineers and Computer Scientists 2017, 15-17 March, 2017, Hong Kong, pp1051-1056

[24] Aravind Prasanth, Sadjyot Biswal, Aman Gupta, and Azan Barodawala, ”Complete Design and Optimization of the Aerodynamics of a FSAE Car using Solid works ANSYS XFLR5,” Lecture Notes in Engineering and Computer Science: Proceedings of The World Congress on Engineering 2016, 29 June - 1 July, 2016, London, U.K., pp961-965

[25] Yung-Lan Yeh, and Cheng-Lin Wu, ”Numerical Simulation of Aerodynamic Improve Schemes for Wind-Loading Solar Power Stent,” Lecture Notes in Engineering and Computer Science: Proceedings of The International MultiConference of Engineers and Computer Scientists 2019, 13-15 March, 2019, Hong Kong, pp547-551

[26] K. Takeda and M. Kato, ”Wind tunnel blockage effects on drag coefficient and wind-induced vibration,” Journal of Wind Engineering and Industrial Aerodynamic, vol. 42 (1-3), pp. 897-908. October 1992.

[27] L. Mckeen, ”Polyamides (Nylons),” Film Properties of Plastics and Elastomers (Fourth Edition), 2017.

[28] M. Vlasblom, ”The manufacture, properties, and applications of high-strength, high-modulus polyethylene fibers,” in Handbook of Properties of Textile and Technical Fibres (Second Edition), 2018.

[29] Y. A Cengel and J. M Cimbala, Fluid Mechanics Fundamentals and Applications, 3rd ed. McGraw-Hill Education, 2014.

[30] P. Panorel and J. Maglasang, ”Experimental and Computational Investigation of Corrugated Dragonfly Airfoil Performance in Small Wind Turbine Applications,” Asia-Pacific Journal of Science, Mathematics and Engineering (APJSME), vol. 4, no. 2, pp. 4-8, 2018.

[31] Dassault Systèmes, SolidWorks Flow Simulation 2012 Technical Reference, SOLIDWORKS 2019, Retrieved from https://www.solidworks.com/

[32] B. Blocken, T. Stathopoulosb, and J. Carmelita, ”CFD simulation of the atmospheric boundary layer: wall function problems,” Atmospheric Environment 41 (2007) 238–252, August 2006.

[33] M. Nagurka and S. Huang, “A Mass-Spring-Damper Model of a Bouncing Ball” in Proceedings of the 2004 American Control Conference, vol. 1, pp. 499-504, 2004.

[34] P. Raju, “Frequency-Domain Vibration Analysis for Characterizing the Dynamic Mechanical Properties of Materials,” American Society for Engineering Education (ASEE), June 1996.

[35] N. Zhu, B. Sparling, and J. P. King, “Comparison of aeroelastic wind tunnel tests and frequency domain analyses of guyed mast dynamic response,” Canadian Journal of Civil Engineering 38(9):984-997, DOI: 10.1139/l10-130, 2011.

[36] T. Irvine, “An Introduction to Shock and Vibration Response Spectra,” In Partnership with enDAQ.com

[37] T. Irvine, “An Introduction to Shock and Vibration Response Spectra Course: The Fourier Transform,” Vibrationdata Publications, 1998.